

Perturbative Wilson loops from unquenched Monte Carlo simulations at weak couplings

Kit Yan Wong

*Simon Fraser University, Department of Physics, 8888 University Drive,
Burnaby, British Columbia, Canada V5A 1S6 and*

*Department of Physics and Astronomy, University of Glasgow, Glasgow, G12 8QQ, United Kingdom**

Howard D. Trottier

*Simon Fraser University, Department of Physics, 8888 University Drive,
Burnaby, British Columbia, Canada V5A 1S6† and*

TRIUMF, 4004 Wesbrook Mall, Vancouver, BC, V6T 2A3, Canada

R. M. Woloshyn

TRIUMF, 4004 Wesbrook Mall, Vancouver, BC, V6T 2A3, Canada

Perturbative expansions of several small Wilson loops are computed through next-to-next-to-leading order in unquenched lattice QCD, from Monte Carlo simulations at weak couplings. This approach provides a much simpler alternative to conventional diagrammatic perturbation theory, and is applied here for the first time to full QCD. Two different sets of lattice actions are considered: one set uses the unimproved plaquette gluon action together with the unimproved staggered-quark action; the other set uses the one-loop-improved Symanzik gauge-field action together with the so-called “asqtad” improved-staggered quark action. Simulations are also done with different numbers of dynamical fermions. An extensive study of the systematic uncertainties is presented, which demonstrates that the small third-order perturbative component of the observables can be reliably extracted from simulation data. We also investigate the use of the rational hybrid Monte Carlo algorithm for unquenched simulations with unimproved-staggered fermions. Our results are in excellent agreement with diagrammatic perturbation theory, and provide an important cross-check of the perturbation theory input to a recent determination of the strong coupling $\alpha_{\overline{\text{MS}}}(M_Z)$ by the HPQCD collaboration.

I. INTRODUCTION

A key ingredient in many high-precision applications of lattice QCD is the use of perturbation theory, in order to match lattice discretizations of actions and observables to their counterparts in continuum QCD. An important example is the determination of the strong coupling $\alpha_{\overline{\text{MS}}}(M_Z)$, where perturbative expansions of short-distance quantities, such as small Wilson loops, can be used to extract the value of the coupling from simulation measurements [1, 2]. Lattice perturbation theory by Feynman diagram analysis is extremely difficult however, because the lattice regulator results in Feynman rules that are exceedingly complicated; moreover, there is a proliferation of diagrams that are not present in the continuum. A further challenge is that these perturbative-matching calculations must generally be carried out at next-to-next-to-leading order (“NNLO,” which is generally equivalent to two-loop Feynman diagrams), if one is to obtain results of a few-percent precision [3].

Although many parts of diagrammatic lattice perturbation theory have been automated with the help of computer codes [3, 4, 5], higher-order calculations remain

very challenging, and very few NNLO lattice calculations have been done (see, e.g., Refs. [2, 6, 7, 8]). The algebraic burden is particularly heavy for the highly-improved actions that are now commonly used in numerical simulations. A particularly important case is the tree-level $O(a^2)$ -improved staggered-quark action (where a is the lattice spacing) [9], together with the $O(a^2)$ -accurate and one-loop Symanzik-improved gluon action [5, 10], both of which are tadpole improved (and which are hereafter collectively referred to as the “asqtad” actions). The “asqtad” actions are currently being used by the MILC collaboration to generate unquenched ensembles with three-flavors of sea quarks [11], which have been used by several groups for a wide variety of physics applications, including quantities requiring higher-order perturbation theory [2, 7, 8].

Given the central role of perturbative matching in lattice QCD, alternatives to diagrammatic perturbation theory are desirable. One approach [12, 13] is to use Monte Carlo simulations at weak couplings, where the theory enters the perturbative phase (at finite volume). Simulation measurements of a particular observable are done at several values of the coupling, and the resulting data are fit to an expansion in the coupling; the fit yields numerical values for the perturbative coefficients, without Feynman diagrams, and with little or no analytic input.

This Monte Carlo approach has been successful in com-

*Present address.

†Permanent address.

puting the perturbation series of a number of quantities in pure gauge theories [12, 13, 14, 15]. In particular, perturbative coefficients for a number of small Wilson loops for the plaquette gluon action were computed to NNLO using this method in Ref. [13], and the results were subsequently reproduced by diagrammatic perturbation theory (see Ref. [3]).

In this paper we make the first applications of this Monte Carlo method to lattice actions with dynamical fermions [16]. The perturbation series of a number of small Wilson loops are computed through NNLO, for two different lattice QCD actions with dynamical staggered quarks: the Wilson plaquette gluon action with the unimproved-staggered quark action, and the “asqtad” actions. The latter calculation is of particular relevance because it provides a consistency check of the NNLO Wilson loop expansions used in the determination of $\alpha_{\overline{\text{MS}}}(M_Z)$ by the HPQCD collaboration, in Ref. [2].

We note that another simulation approach to lattice perturbation theory has also been developed, based on an explicit perturbative expansion of the simulation equations themselves [17], and has recently been applied to (unimproved) lattice actions with dynamical fermions [18].

The Monte Carlo method considered here has the advantage that it can be done using conventional simulation codes, although it is very advantageous to adopt twisted boundary conditions (TBC) [5, 19, 20, 21, 22] in order to eliminate zero modes, and to suppress nonperturbative finite-volume effects due to transitions between $Z(3)$ phases [13]; fortunately, TBC can be implemented in existing simulation codes with relatively little effort.

This simulation approach to unquenched perturbation theory is also very efficient, since the simulations can be done on very small lattices (8^4 volumes are used here), thanks to the use of TBC. The simulations are also done here for different numbers n_f of dynamical fermions, which explicitly demonstrates that the data are sensitive to the n_f -dependence of the perturbative coefficients.

Although small Wilson loops are the simplest observables for perturbative analysis by Monte Carlo simulations, because they are such ultraviolet quantities (as well as being gauge invariant), the studies presented here nonetheless provide important benchmarks for future applications to other quantities; for instance, similar methods were used to analyze the static-quark propagator in pure-gauge backgrounds in Ref. [13], and the Fermilab heavy-quark propagator was analyzed in Ref. [14].

While the expansion coefficients can be extracted with far less effort from Monte Carlo simulations, care must be taken to control all of the systematic uncertainties, in order to reliably extract the small part of the signal corresponding to the higher-order terms in the perturbative expansion. It is also crucial to use an expansion in a renormalized coupling, rather than in the bare lattice coupling $\alpha_{\text{lat}} = g^2/(4\pi)$, for which perturbation theory is very poorly convergent [23]. We use an expansion in the coupling $\alpha_V(q^*)$ defined by the static potential, along

with an estimate of the optimal scale q^* for a given quantity [23, 24]. Although one can in principle define the renormalized coupling α_V at a given bare lattice coupling α_{lat} from simulation measurements of the static potential, we rely here instead on existing NNLO determinations of the relationship from diagrammatic perturbation theory [7].

We did simulations at couplings $\alpha_V \lesssim 0.1$, hence statistical and systematic errors must be much less than $\max(\alpha_V^3) \sim 10^{-3}$, for determination of the third-order coefficients. The ensemble sizes were chosen in order to reduce the statistical errors to the desired level. There are four major sources of systematic error in the simulation algorithms and in the data analysis: i) transitions between the $Z(3)$ center phases of the gauge field action; ii) finite step-size errors in the simulation equations; iii) other algorithmic systematics, such as the precision of the matrix inversion; and iv) fitting and truncation errors in the perturbative expansion.

In this study simulations were done with TBC to suppress transition between the center phases, as indicated above. To eliminate the finite step-size errors we pursued one of two strategies: in the case of the unimproved actions, we used the rational hybrid Monte Carlo algorithm (RHMC) [25, 26]; for the “asqtad” actions we used the R algorithm [27], and did simulations at several different molecular-dynamics step sizes, the results of which were extrapolated to zero step size. To extract the perturbative coefficients the data were analyzed using constrained curve fitting techniques [28], which provide an elegant procedure for incorporating our *a priori* expectation that the perturbative expansion is well behaved, and which readily allow the maximum amount of information to be extracted from the data.

The rest of the paper is organized as follows. The actions and simulation parameters are detailed in Sect. II, along with the perturbation theory input which we use to extract the renormalized coupling α_V at a given bare lattice coupling, from the simulation data. A detailed analysis of the systematic uncertainties is presented in Sect. III, including the use of TBC to control finite-volume effects. Results for the two actions are reported in Sect. IV, and are compared with NNLO diagrammatic perturbation theory. Conclusions and prospects for further work are presented in Sect. V.

II. ACTIONS AND SIMULATION PARAMETERS

A. Perturbative expansions

We have done unquenched simulations for two sets of actions: the first set used the unimproved Wilson plaquette action with unimproved-staggered fermions, while the second set used $O(a^2)$ -improved gluon and staggered-quark actions. We provide the simulation parameters and perturbation theory input for each set of actions in the

two following subsections.

A basic input parameter for the simulations is the bare lattice coupling $\alpha_{\text{lat}} = g^2/(4\pi)$, related to the usual simulation parameter β in the case of the Wilson plaquette action, for example, according to $\beta \equiv 6/g^2 = 6/(4\pi\alpha_{\text{lat}})$. However the bare coupling is not suitable for perturbative expansions [23] and we use instead a renormalized coupling $\alpha_V(q)$, defined by the static potential according to [23, 24]

$$V(q) \equiv -\frac{4}{3} \frac{4\pi\alpha_V(q)}{q^2}. \quad (1)$$

A (truncated) perturbative expansion for the logarithm of a Wilson loop of size $R \times T$ is used, owing to the perturbative perimeter law,

$$-\frac{1}{2(R+T)} \ln W_{RT} \approx \sum_{n=1}^N c_{n;RT} \alpha_V^n(q_{RT}^*), \quad (2)$$

where N is the order at which the series is truncated. We aim to measure the coefficients through third-order, hence fits must be done with $N \geq 3$. The characteristic scale q_{RT}^* for each observable is determined according to the BLM method (which estimates the typical momentum carried by a gluon in leading-order diagrams) [23, 24].

The connection between the simulation input α_{lat} and the α_V coupling is therefore required. Although it is possible, in principle, to extract this relation by directly measuring the static-quark potential in Monte Carlo simulations, the connection has already been computed in diagrammatic perturbation theory through NNLO for a

variety of actions, including those we consider here, in Ref. [7]. We use the results of Ref. [7] to provide the three leading orders of the expansion for the 1×1 plaquette, as well as the scales q_{RT}^* for all the Wilson loops (the later only requires a relatively straightforward one-loop calculation).

The diagrammatic input provided by the expansion of the 1×1 loop simplifies our analysis, and still allows for highly-nontrivial applications of the Monte Carlo method; here we demonstrate the utility of the method by computing the NNLO perturbative expansions of several larger Wilson loops, and thereby also provide a valuable consistency check of the NNLO diagrammatic calculations which were used to obtain $\alpha_{\overline{\text{MS}}}(M_Z)$ in Refs. [2, 7].

Given this input from diagrammatic perturbation theory, the Monte Carlo method proceeds as follows. Simulations are done at several small values of the bare coupling α_{lat} (at which the lattice theory is in the perturbative phase at a given finite volume). For each bare coupling one measures the average plaquette $\langle W_{11} \rangle_{\text{MC}}$, whose perturbative expansion is assumed, and the quantities of interest, whose perturbative expansions are to be determined; in our case these latter quantities are larger Wilson loops, $\langle W_{RT} \rangle_{\text{MC}}$. The numerical value of the renormalized coupling α_V at the scale q_{11}^* is obtained by substituting the measured value $\langle W_{11} \rangle_{\text{MC}}$ into its known third-order expansion. Once the numerical value of $\alpha_V(q_{11}^*)$ has been determined, the couplings at the other relevant scales q_{RT}^* can be computed using the universal second-order beta function, plus the known third-order correction in the V scheme [29], according to

$$\alpha_V(q) = \frac{4\pi}{\beta_0 \ln(q^2/\Lambda_V^2)} \left[1 - \frac{\beta_1}{\beta_0^2} \frac{\ln[\ln(q^2/\Lambda_V^2)]}{\ln(q^2/\Lambda_V^2)} + \frac{\beta_1^2}{\beta_0^4 \ln^2(q^2/\Lambda_V^2)} \left(\left(\ln[\ln(q^2/\Lambda_V^2)] - \frac{1}{2} \right)^2 + \frac{\beta_{2V}\beta_0}{\beta_1^2} - \frac{5}{4} \right) \right], \quad (3)$$

where $\alpha_V(q_{11}^*)$ is traded for the intrinsic scale Λ_V at the given bare coupling. The beta-function coefficients are $\beta_0 = 11 - \frac{2}{3}n_f$, $\beta_1 = 102 - \frac{38}{3}n_f$, and $\beta_{2V} = 4224.18 - 746.006n_f + 20.8719n_f^2$. Fits to the expansion Eq. (2) then yield the perturbative coefficients for the larger Wilson loops; details on the fitting procedure are described in Sect. III D.

B. Unimproved actions

The first set of actions we consider are the Wilson plaquette gluon action,

$$S_{\text{glue}}^{\text{unimp}} = \beta \sum_{x:\mu<\nu} (1 - P_{\mu\nu}), \quad (4)$$

where $P_{\mu\nu}$ is the 1×1 plaquette and $\beta = 6/g^2$, together with the unimproved staggered-quark action

$$S_{\text{stagg}}^{\text{unimp}} = \sum_x \bar{\chi}(x) \left(\sum_{\mu} \eta_{\mu}(x) \Delta_{\mu} + m_0 \right) \chi(x), \quad (5)$$

where Δ_{μ} is the standard lattice derivative, and $\eta_{\mu}(x) = (-1)^{x_1+\dots+x_{\mu-1}}$ is the usual staggered-quark phase.

Two sets of simulations were done for the unimproved actions; the simulation parameters are summarized in Table I. One set was done for a single dynamical flavor, $n_f = 1$, and another was done for three degenerate dynamical flavors, $n_f = 3$. In each case, simulations were done for seven values of the bare coupling, with bare-quark mass $m_0 a = 0.2$, on 8^4 lattices with twisted boundary conditions (the boundary conditions

Number of flavors: $n_f = 1$						
β	$\alpha_{\text{lat}} = 6/4\pi\beta$	$\langle W_{11} \rangle$	Measurements	Acc. Rate	$\alpha_V(q_{11}^*)$	$a\Delta_V$
11.0	0.04341	0.805569(41)	849	92%	0.05574	2.1×10^{-5}
13.5	0.03537	0.843964(34)	902	90%	0.04292	9.1×10^{-6}
16.0	0.02984	0.869561(26)	992	87%	0.03496	4.0×10^{-7}
19.0	0.02513	0.890999(21)	981	81%	0.02860	9.2×10^{-9}
24.0	0.01989	0.914413(16)	1066	69%	0.02198	1.7×10^{-11}
32.0	0.01492	0.936259(11)	1180	58%	0.01605	7.2×10^{-16}
47.0	0.01016	0.956886(7)	1261	53%	0.01067	4.2×10^{-24}

Number of flavors: $n_f = 3$						
β	$\alpha_{\text{lat}} = 6/4\pi\beta$	$\langle W_{11} \rangle$	Measurements	Acc. Rate	$\alpha_V(q_{11}^*)$	$a\Delta_V$
11.0	0.04341	0.807064(36)	821	89%	0.05551	3.9×10^{-6}
13.5	0.03537	0.844847(26)	641	86%	0.04283	1.1×10^{-6}
16.0	0.02984	0.870205(21)	740	84%	0.03490	2.9×10^{-8}
19.0	0.02513	0.891387(18)	738	77%	0.02859	3.8×10^{-10}
24.0	0.01989	0.914647(13)	791	66%	0.02197	2.7×10^{-13}
32.0	0.01492	0.936402(10)	840	56%	0.01605	2.5×10^{-18}
47.0	0.01016	0.956950(6)	902	52%	0.01066	8.5×10^{-28}

TABLE I: Simulation parameters for the unimproved plaquette gluon action with the unimproved staggered-quark action. Two different sets of simulations were done for the indicated number of flavors; in both cases 8^4 lattices with twisted boundary conditions were used, with bare-quark mass $m_0 a = 0.2$. The RHMC algorithm was used with step size $\Delta t = 0.01$, with 50 molecular-dynamics steps per trajectory; the table shows the acceptance rate for the accept/reject step at the end of each trajectory.

Loop	q_{RT}^*	Loop	q_{RT}^*
1×1	3.40	2×2	2.65
1×2	3.07	2×3	2.56
1×3	3.01	3×3	2.46

TABLE II: The optimal momentum scales q_{RT}^* for selected $R \times T$ Wilson loops for the unimproved actions [7].

are discussed in Sect. III A). The configurations for these actions were generated using the RHMC algorithm, described in more detail in Sect. III B; we used a time-step $\Delta t = 0.01$ with 50 molecular-dynamics steps between accept/reject tests. Based on an autocorrelation analysis, described in Sect. III C, 40 trajectories were skipped between measurements.

For the unimproved actions the expansion coefficients of the average plaquette to NNLO are given by [7, 30]

$$\begin{aligned}
c_{1;11} &= 1.04720(0), \\
c_{2;11} &= -1.2467(2) - 0.06981(5)n_f, \\
c_{3;11} &= -1.778(7) + 0.464(27)n_f + 0.00485(0)n_f^2, \quad (6)
\end{aligned}$$

where the uncertainties in the coefficients are statistical errors which arise from numerical integration of the multi-loop Feynman diagrams using a Monte Carlo technique (the error of “0” in $c_{1;11}$ indicates that the integration error is in the sixth digit in that case). The relevant scales for the Wilson loops are given in Table II.

C. Improved actions

The one-loop Symanzik-improved gluon action [5, 10] we use follows Refs. [11, 31] for tadpole improvement

$$\begin{aligned}
S_{\text{glue}}^{\text{imp}} &= \beta_{\text{pl}} \sum_{x;\mu<\nu} (1 - P_{\mu\nu}) + \beta_{\text{rt}} \sum_{x;\mu\neq\nu} (1 - R_{\mu\nu}) \\
&+ \beta_{\text{pg}} \sum_{x;\mu<\nu<\sigma} (1 - C_{\hat{\mu},\pm\hat{\nu},\pm\hat{\sigma}}), \quad (7)
\end{aligned}$$

where $R_{\mu\nu}$ is the 1×2 rectangle, $C_{\mu\nu\sigma}$ is the $1 \times 1 \times 1$ “corner cube” (see Ref. [11]), and where the couplings are given by

$$\begin{aligned}
\beta_{\text{pl}} &= \frac{10}{g^2}, \quad \beta_{\text{rt}} = -\frac{\beta_{\text{pl}}}{20u_0^2}(1 + 0.4805\alpha_s), \\
\beta_{\text{pg}} &= -\frac{\beta_{\text{pl}}}{u_0^2}0.03325\alpha_s, \quad (8)
\end{aligned}$$

with α_s here defined by the (first-order accurate) expression

$$\alpha_s \equiv -4 \ln(u_0)/3.0684. \quad (9)$$

The one-loop couplings in $S_{\text{glue}}^{\text{imp}}$ correspond to the average-plaquette definition of the gluon mean field

$$u_0 \equiv (W_{11})^{1/4}. \quad (10)$$

The tree-level $O(a^2)$ -accurate improved staggered-quark action we simulate was derived in Ref. [9], and

β	Input u_0	Measured u_0	α_{lat}	$\alpha_V(q_{11}^*)$	$a\Lambda_V$	Measurements
9.5	0.91690	0.916922(98)	0.08377	0.12709	5.8×10^{-2}	461,457,836,1335
11.0	0.93166	0.931687(73)	0.07234	0.10113	2.0×10^{-2}	281,633,1090,1038
13.5	0.94704	0.946986(55)	0.05895	0.07604	3.2×10^{-3}	290,635,1122,1078
16.0	0.95661	0.956614(53)	0.04974	0.06106	5.0×10^{-4}	296,634,1145,1100
19.0	0.96433	0.964311(38)	0.04188	0.04951	5.5×10^{-5}	298,643,1123,1172
24.0	0.97243	0.972453(29)	0.03316	0.03765	1.3×10^{-6}	308,645,1191,1113
32.0	0.97978	0.979785(23)	0.02487	0.02727	3.3×10^{-9}	315,652,1205,1204
47.0	0.98652	0.986526(15)	0.01693	0.01797	3.8×10^{-14}	215,709,1227,963
80.0	0.99220	0.992208(13)	0.00995	0.01029	5.3×10^{-25}	472,489,974,1527

TABLE III: Simulation parameters for the “asqtad” actions on 8^4 lattices with twisted boundary conditions. The number of flavors is $n_f = 1$, with bare-quark mass $m_0 a = 0.1$. Simulations at each bare lattice coupling were done at four values of the R -algorithm step-size, $\Delta t = 0.005, 0.01, 0.02$, and 0.03 . The measured u_0 and $\alpha_V(q_{11}^*)$ are only shown for the ensembles with $\Delta t = 0.005$. The number of measurements at each of the four step sizes is given.

Loop	q_{RT}^*	Loop	q_{RT}^*
1×1	3.33	2×2	2.58
1×2	3.00	2×3	2.48
1×3	2.93	3×3	2.37

TABLE IV: The optimal momentum scales q_{RT}^* for selected $R \times T$ Wilson loops for the “asqtad” actions [7].

is also used in the three-flavor simulations by the MILC collaboration [11]

$$S_{\text{stag}}^{\text{imp}} = \sum_x \bar{\chi}(x) \left[\sum_{\mu} \eta_{\mu}(x) \left(\Delta'_{\mu} - \frac{a^2}{6} \Delta_{\mu}^3 \right) + m_0 \right] \chi(x); \quad (11)$$

see Ref. [9] for the definition of the “smeared” derivative operator Δ'_{μ} . Tadpole improvement of $S_{\text{stag}}^{\text{imp}}$ is defined by replacing each link U_{μ} in the action by \tilde{U}_{μ}/u_0 , but only after adjacent pairs of identical links ($U_{\mu}^{\dagger} U_{\mu} = I$) are eliminated; the tadpole weights for the individual link paths in the quark action were also detailed by the MILC collaboration [11].

Simulations were done for the “asqtad” actions only for a single dynamical flavor, $n_f = 1$. Ensembles were generated at nine values of the bare coupling, on 8^4 lattices and with bare-quark mass $m_0 a = 0.1$; simulation parameters are given in Table III.

The R algorithm was used in these simulations, and ensembles were generated at each bare coupling at four different molecular-dynamics step sizes, $\Delta t = 0.005, 0.01, 0.02$, and 0.03 , with the number of steps per trajectory in the four cases given by 100, 50, 25, and 15, respectively. The measured Wilson loop data are extrapolated to $\Delta t = 0$ at each bare coupling using constrained curve fitting (cf. Sect. III D). The simulation value of the tadpole factor u_0 is determined self-consistently at each bare coupling by iteration during the thermalization process; the “final” input value was verified for consistency with the final measured value of u_0 , as shown in Table III. Based on an autocorrelation analysis, described in Sect. III C, we skipped 20 trajectories between mea-

surements.

For the “asqtad” actions the expansion coefficients of the average plaquette to NNLO are given by [7, 30]

$$\begin{aligned} c_{1;11} &= 0.76710(0), \\ c_{2;11} &= -0.5945(2) - 0.07391(2)n_f, \\ c_{3;11} &= -0.589(38) + 0.600(2)n_f + 0.00774(0)n_f^2, \end{aligned} \quad (12)$$

The relevant scales for the Wilson loops are given in Table IV.

III. SYSTEMATIC EFFECTS

The various systematic effects which must be controlled in order to extract higher-order expansion coefficients were enumerated in the Introduction, and in the following four subsections we consider these in turn.

A. $Z(3)$ phases and twisted boundary conditions

The $SU(3)_{\text{color}}$ gauge-field action is invariant under the transformation

$$U_{\mu}(x) \rightarrow z U_{\mu}(x), \quad \forall x \ni x \cdot \hat{\mu} = \text{constant}, \quad (13)$$

where $z \in [1, e^{i2\pi/3}, e^{i4\pi/3}]$ is an element of the center-subgroup $Z(3)$. Although all closed Wilson loops are invariant under this transformation, the Polyakov line in the μ direction is sensitive to the phase; moreover, the perturbative expansion of Wilson loops can be spoiled by the formation of domains of different center phases [12]. While the fermion action breaks the center symmetry, the action “cost” for reaching different phases, at the lattice volume considered here, is too small to prevent frequent transitions between phases, at least when periodic boundary conditions (PBC) are used. This can be seen in Fig. 1, where a scatter plot and run-time history of the “temporal” Polyakov line are shown for the unimproved actions with PBC, on a 4^4 lattice at $\beta = 16$, well into the deconfined phase of the theory.

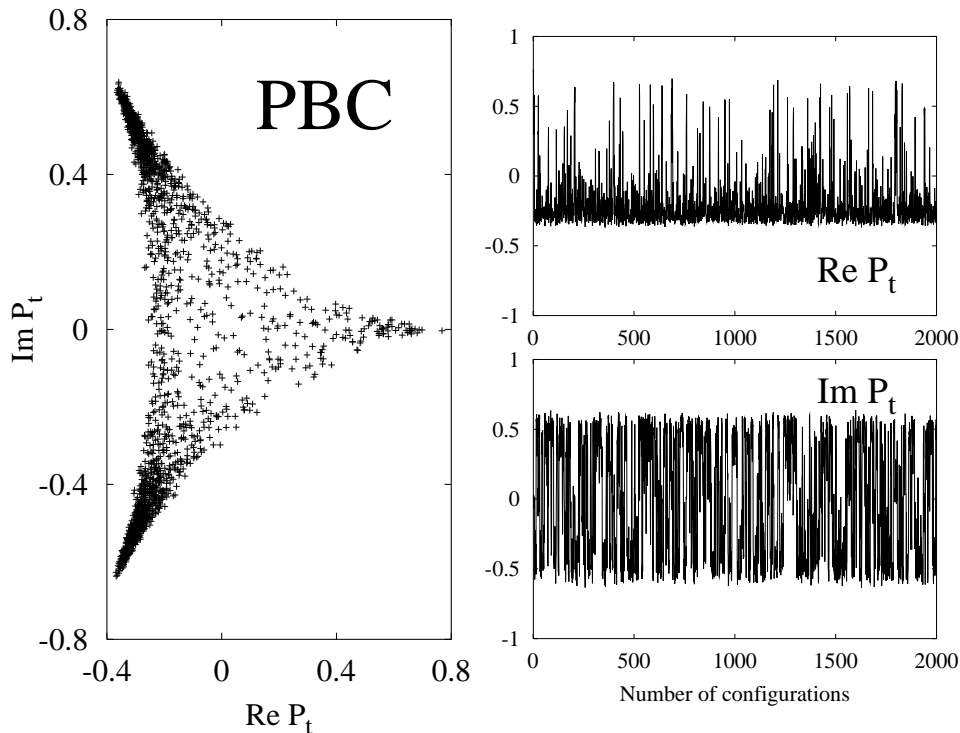


FIG. 1: Scatter plot and run-time history of the “temporal” Polyakov loop P_t on a 4^4 lattice at $\beta = 16$, using periodic boundary conditions. Results are shown for the unimproved actions using the RHMC algorithm, with $n_f = 1$, and bare-quark mass $m_0 a = 0.2$; 100 trajectories were skipped between measurements. The simulations were started with all links set to the identity, $U_\mu(x) = I$, and the history is shown starting from this initial configuration.

Although the scatter plot shows that the action with dynamical fermions has a preference for configurations near the non-trivial phases $z = e^{i2\pi/3}$ and $z = e^{i4\pi/3}$ (despite the fact that the simulation was started with all links set to the identity), owing to the breaking of the $Z(3)$ symmetry, transitions between the various phases occur frequently, which would prevent the extraction of perturbative expansions, except on very large lattices [13].

Fortunately, the $Z(3)$ transitions can be largely eliminated by using twisted boundary conditions (TBC) [13], which can be easily implemented using existing simulation codes. In the case of the gauge fields, there is no change to the link variables inside the lattice, and link variables across the twisted lattice boundaries are computed according to

$$U_\mu(x + L\hat{\nu}) = \Omega_\nu U_\mu(x) \Omega_\nu^\dagger, \quad (14)$$

where L is the lattice length, and the Ω_ν are a set of constant “twist” matrices which obey the algebra [5]

$$\Omega_\mu \Omega_\nu = z \Omega_\nu \Omega_\mu, \quad \Omega_\nu^3 \propto I. \quad (15)$$

The gauge action and observables are therefore periodic with TBC, but with period $3L$, and with the important additional benefit that zero modes are eliminated [5].

Twists must be applied across at least two boundaries, else the effect of the twist matrix can be removed by a field redefinition. We choose to impose twists across all three “spatial” lattice boundaries, with ordinary periodic boundary conditions across the “temporal” boundary [13]. The following explicit representation of the twist matrices was used in our simulations

$$\Omega_x = \begin{bmatrix} 0 & 1 & 0 \\ 0 & 0 & 1 \\ 1 & 0 & 0 \end{bmatrix}, \quad \Omega_y = \begin{bmatrix} e^{-i2\pi/3} & 0 & 0 \\ 0 & 1 & 0 \\ 0 & 0 & e^{+i2\pi/3} \end{bmatrix},$$

$$\Omega_z = \Omega_x^2 \Omega_y = \begin{bmatrix} 0 & 0 & e^{-i2\pi/3} \\ 1 & 0 & 0 \\ 0 & e^{+i2\pi/3} & 0 \end{bmatrix}. \quad (16)$$

To apply twists to the unquenched theory the quark field fields $\chi(x)$ must become 3×3 color matrices [20, 21]; these additional fermionic degrees-of-freedom amount to a new set of three degenerate “flavors” (Parisi introduced the term “smells” [20], to distinguish these copies from physical quark flavors). To compute the fermion fields across the twisted lattice boundaries one then imposes the boundary conditions

$$\chi(x + L\nu) = e^{i\pi/3} \Omega_\nu \chi(x) \Omega_\nu^\dagger, \quad (17)$$

where the phase $e^{i\pi/3}$ makes the quark field anti-periodic

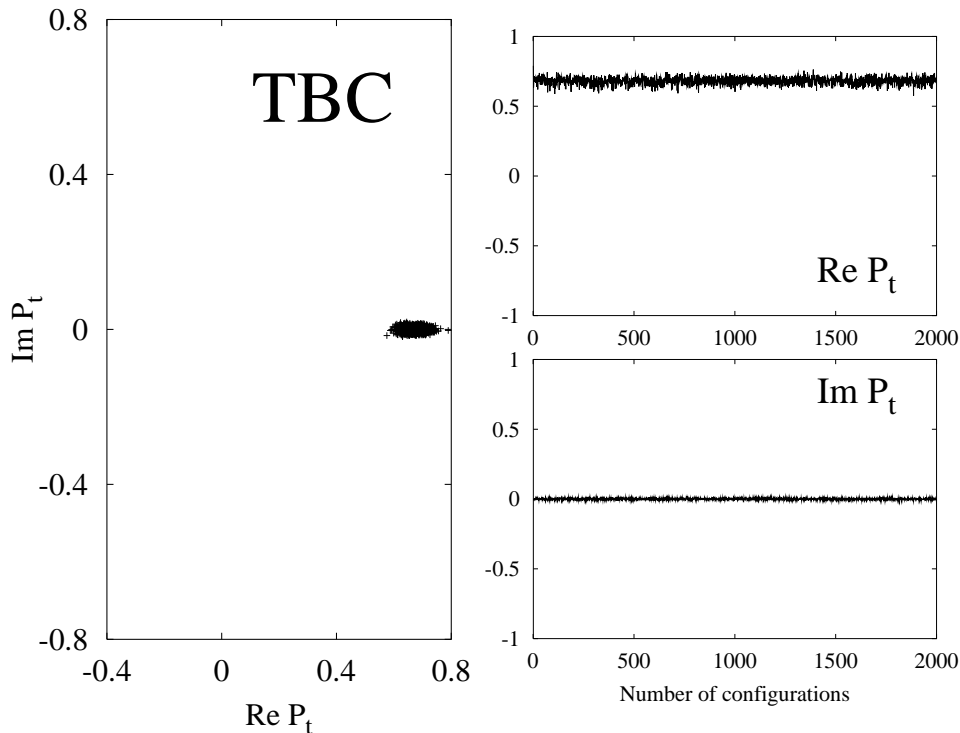


FIG. 2: Unimproved action scatter plot and run-time history, with the same simulation parameters as in Fig. 1, but here using twisted boundary conditions (TBC) in the three “spatial” directions.

(on intervals $3L$), thereby eliminating its zero modes as well.

As a result of the three-fold increase in the number of components of the quark field, unquenched simulations using TBC will be roughly three times as expensive as simulations using PBC for the same action (although this cost is far offset by the reduction in finite volume effects). To compensate for the extra fermion copies we include an additional factor of $1/3$ in the fermion force term (on top of the $1/4$ to reduce the four staggered “tastes” to a single effective quark flavor); we therefore continue to use n_f to denote the total number of quark “flavors.”

Figure 2 shows a scatter plot and run-time history of the temporal Polyakov for simulations done with TBC, using the same simulation parameters that were used with PBC to generate Fig. 1. The suppression of $Z(3)$ transitions when TBC are used is striking. In fact, we have generated about one million configurations with TBC (at a larger volume $V = 8^4$), and not a single transition away from the “trivial” $Z(3)$ phase has been observed.

B. Simulation algorithms

Dynamical simulations with staggered quarks have generally been done with the R algorithm. The major disadvantage of this algorithm is that measured quanti-

ties have leading $O(\Delta t^2)$ errors [27], where Δt is the step-size in the molecular-dynamics evolution equations. The step-size errors cannot be corrected by a Monte Carlo accept/reject procedure, because the fermion force is not computed explicitly in the R algorithm, rather a noisy estimator is used. This leads to a large change in the system energy during the molecular-dynamics updates, making the acceptance rate small if one would impose a Monte Carlo accept/reject step at the end of the evolution. Therefore simulations are generally done at several values of Δt , and the results are extrapolated to zero step size. This is the method we use to simulate the “asqtad” actions, for which ensembles were generated at four values of Δt at each bare lattice coupling (see Table III). The Wilson loop data at a given bare coupling were fit to an expansion in Δt , including terms up to $O(\Delta t^6)$, excluding the linear term (constrained-curve fits were used, with priors for each term in the fit set to 0 ± 5 , see Sect. III D). Some typical results for the step-size extrapolations are shown in Fig. 3.

Step-size errors can be eliminated using the rational hybrid Monte Carlo (RHMC) algorithm to handle the fractional powers of the staggered matrix [25, 26]. In the RHMC algorithm the fermion force for staggered quarks is computed explicitly by approximating the $(n_f/4)$ -th root (or the $(n_f/12)$ -th root in the case of TBC) of the fermion matrix with a rational function (and retaining only even-site couplings in $M^\dagger M$, as usual, to avoid a

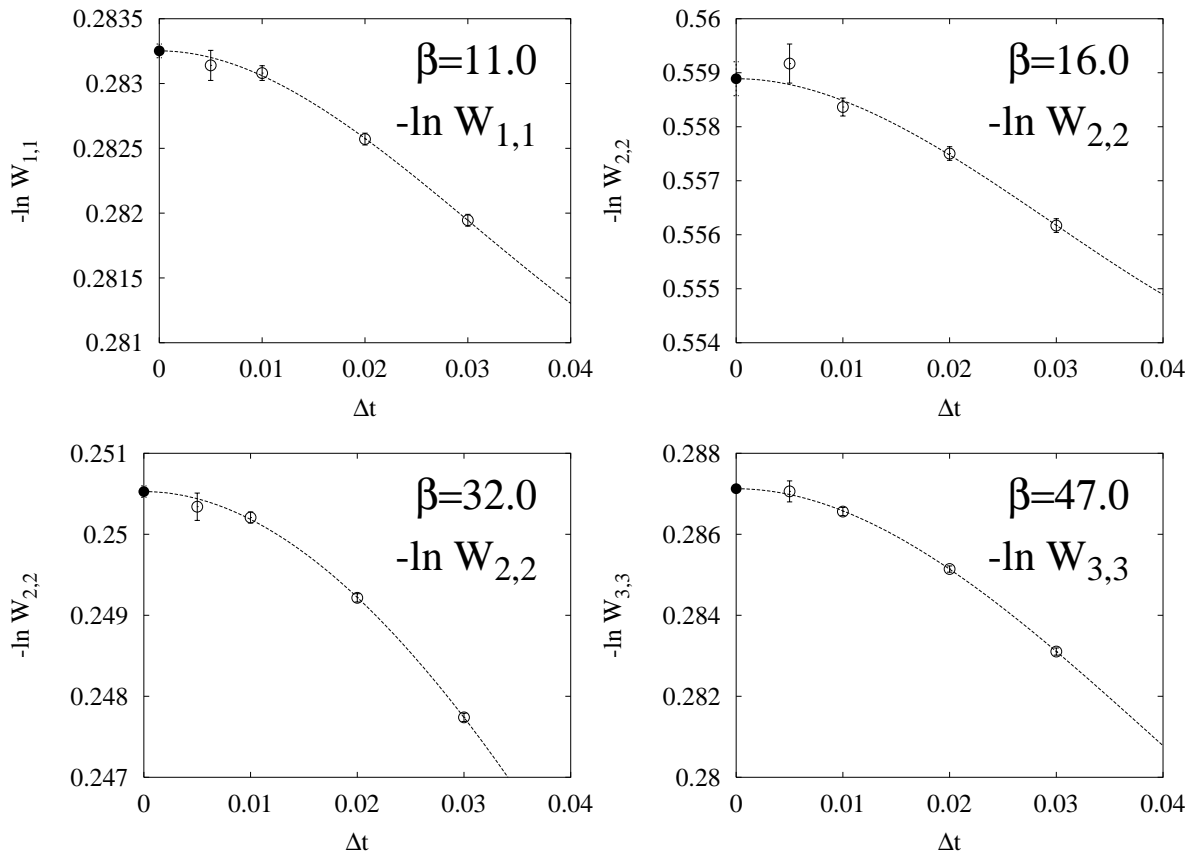


FIG. 3: Representative step-size extrapolations of the R -algorithm simulation results for the “asqtad” actions.

further redoubling of fermion degrees-of-freedom). This allows an explicit computation of the force term, hence the step-size errors can be corrected efficiently using a Monte Carlo accept/reject step.

We tested the efficiency of the RHMC algorithm by applying rational function approximations of various degrees $[N_{\text{rat}}, N_{\text{rat}}]$, that is, the numerator and denominator are taken to be polynomials of degree N_{rat} . This was done to approximate both $x^{-1/12}$ (for TBC with $n_f = 1$) and $x^{-1/4}$ (for TBC with $n_f = 3$), in the interval $x \in [\lambda_{\text{min}}, \lambda_{\text{max}}]$, where we estimate the lower and upper bounds on the eigenvalue spectrum of $M^\dagger M$ from the free-field values, $\lambda_{\text{min}} = (2m_0 a)^2$ and $\lambda_{\text{max}} = 64 + (2m_0 a)^2$, respectively.

Results for degrees $N_{\text{rat}} = 6, 8, 10$ and 12 are shown in Fig. 4, for two values of the bare coupling. The maximum error in the rational approximation, over the requisite eigenvalue range, falls below about 10^{-5} at around $N_{\text{rat}} = 10$, and it appears as well that at larger orders there is little change in the ensemble averages of the plaquette, within the statistical errors. We therefore use $N_{\text{rat}} = 10$ throughout the rest of this study (on the other hand, only a 5% difference in performance is observed for each additional order in the approximation). The RHMC code is found to be about two-times slower com-

pared to the R algorithm, using the same Δt and number of molecular-dynamics steps. Given that the acceptance rate varies from about 90% at $\beta = 11$ to about 50% at $\beta = 47$ (see Table I), we conclude that the RHMC algorithm is about 2–4 times more expensive; however, we generated four sets of ensembles at different step-sizes for the R algorithm, in order to extrapolate to $\Delta t = 0$, hence we find that the two algorithms are, in practice, of comparable cost for unimproved-staggered quarks.

C. Other algorithmic systematics

We have explicitly computed autocorrelation times for the simulation data. This is important because gauge-field fluctuations are suppressed at weak couplings, which should lead to longer autocorrelation times as the coupling is decreased; moreover, little information on autocorrelations in the weak-coupling phase is available from other studies. The autocorrelation for a set of measurements \mathcal{O}_i of some observable is defined, as usual, by

$$\text{Corr}(N_{\text{skip}}) = \frac{\sum_i (\mathcal{O}_i - \bar{\mathcal{O}})(\mathcal{O}_{i+N_{\text{skip}}} - \bar{\mathcal{O}})}{\sum_i (\mathcal{O}_i - \bar{\mathcal{O}})^2}, \quad (18)$$

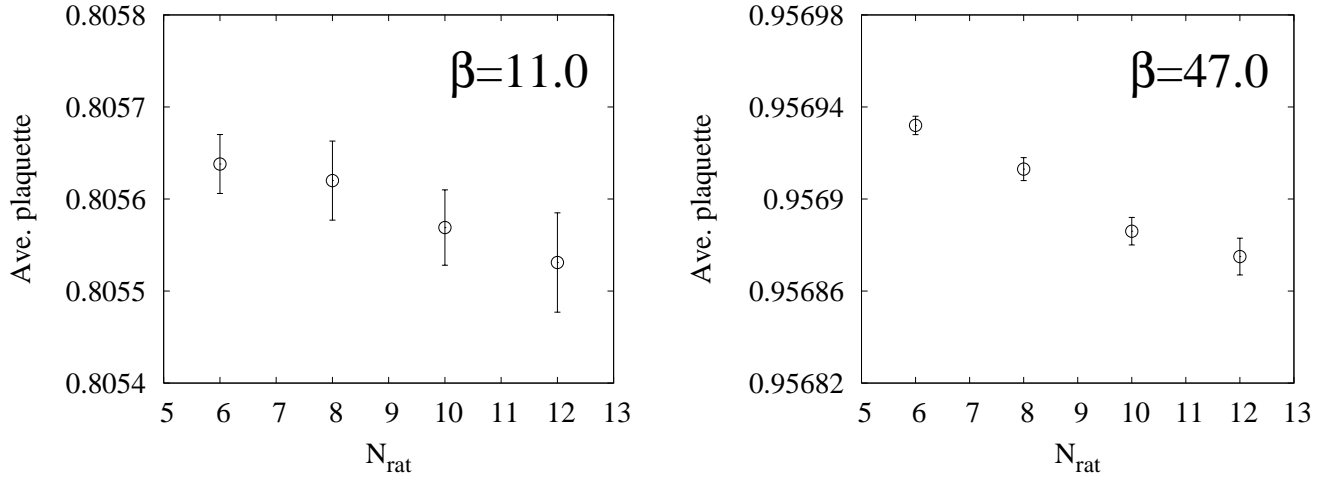


FIG. 4: Average plaquettes computed using different degrees N_{rat} of the polynomials in the rational approximation to the unimproved staggered-quark force term. Results are shown for $n_f = 1$ at $\beta = 11$ and 47.

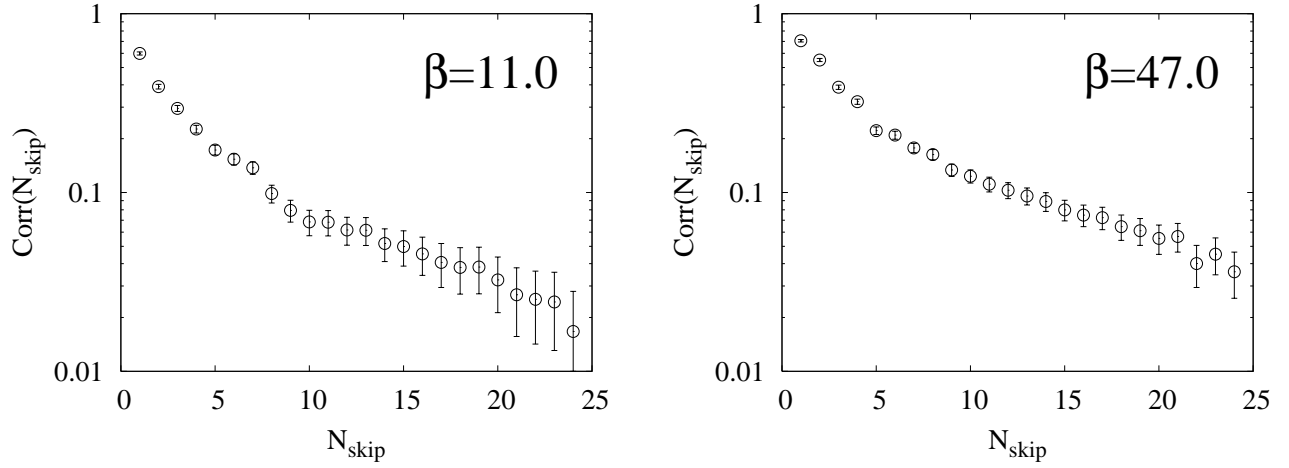


FIG. 5: Autocorrelation plots for the 3×3 loops for the “asqtad” actions, at two different couplings. Configurations were generated by the R algorithm, with $\Delta t = 0.01$ and 50 molecular-dynamics steps per trajectory.

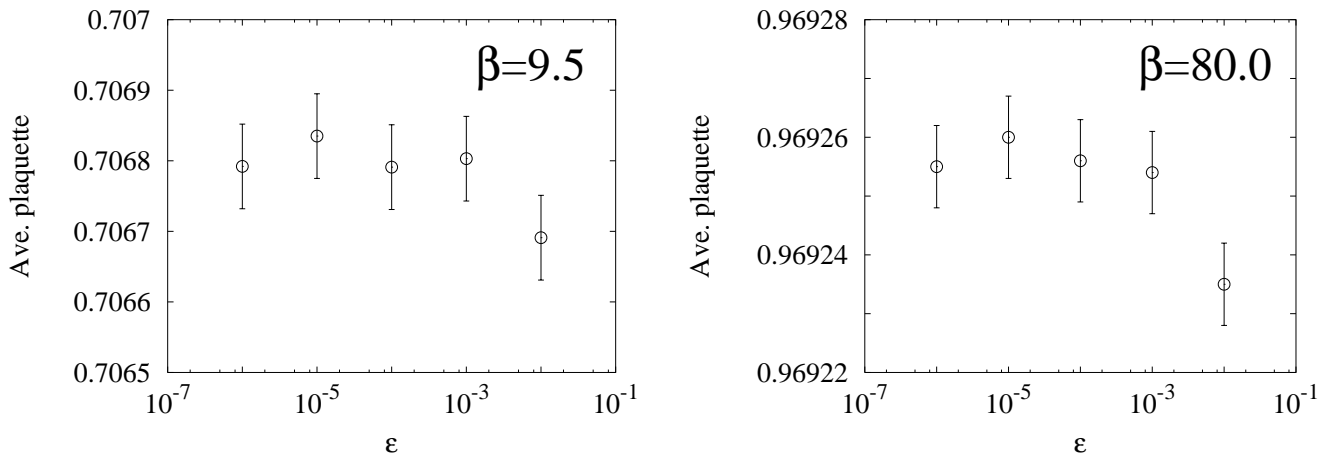


FIG. 6: Average plaquettes computed with different convergence criteria for the matrix inversion by the stabilized bi-conjugate-gradient method. Results are shown for the “asqtad” actions at two couplings.

where N_{skip} is the number of “skipped” trajectories, and where the autocorrelation time τ is estimated from $\text{Corr}(N_{\text{skip}}) \sim e^{-N_{\text{skip}}/\tau}$. The autocorrelation time is observable-dependent, and one generally expects to have longer autocorrelation times for a “larger” observable, such as a larger Wilson loop. Figure 5 shows the autocorrelation function for the 3×3 Wilson loop, the largest considered here, at two couplings, for the “asqtad” actions. Note that the autocorrelation time is longer for the larger value of β , as expected. Based on these results, we have chosen to skip 20 trajectories between measurements for the “asqtad” simulations. In the case of the RHMC algorithm that was used for the unimproved action, where the lowest acceptance rate is about 50%, 40 trajectories were skipped between measurements.

Another source of systematic error is the accuracy of the matrix inversion, which affects both the R algorithm and the RHMC algorithm. The Monte Carlo accept/reject step in the RHMC algorithm cannot remove this error since matrix inversions are also required in computing the action for this setp. Matrix inversions $(M^\dagger M)^{-1}\phi = x$ were done by the stabilized bi-conjugate-gradient method, with a convergence criterion $\|(M^\dagger M)x - \phi\| < \epsilon$. We tested the precision of the inversion by comparing ensemble averages computed with different values of ϵ . Results are shown in Fig. 6 for the average plaquette for the “asqtad” actions. Results are consistent within statistical errors for $\epsilon \lesssim 10^{-3}$; we used $\epsilon = 10^{-5}$ in the production runs.

An additional systematic error arises from propagation of the uncertainties in the couplings $\alpha_V(q_{11}^*)$, which are due to the statistical errors in the measured values of the 1×1 plaquette, from which the couplings are extracted. The errors in $\alpha_V(q_{11}^*)$ propagate through to the couplings $\alpha_V(q_{RT}^*)$ that are used in the fits to the larger Wilson loops. This could be accounted for by including the associated uncertainty in the scale parameters Λ_V (cf. (Eq. 3)), in the augmented χ^2 that is used in the Bayesian analysis (see Sect. III D below). We have instead propagated the error in the coupling by using a first-order approximation to the perturbative expansions (which is adequate for this purpose), $-\ln W_{RT}/2(R+T) \approx c_{1;RT} \alpha_V(q_{RT}^*)$. This implies that the statistical uncertainty $\Delta[\ln W_{11}]_{\text{MC}}$ in the 1×1 loop “induces” an additional uncertainty $\Delta[\ln W_{RT}]_{\text{induced}}$ in the $R \times T$ loop, beyond its own statistical error, through the coupling, given by

$$\Delta[\ln W_{RT}]_{\text{induced}} \approx \frac{\ln W_{RT}}{\ln W_{11}} \times \Delta[\ln W_{11}]_{\text{MC}}. \quad (19)$$

It turns out that the simulation error in $\ln W_{RT}$ grows more rapidly than $-\ln W_{RT}$ itself, as the loop gets larger, hence the “induced” error becomes less important for larger loops; a representative comparison of the errors for various loops is shown in Table V. The sum of the two correlated errors (statistical and “induced”) is used in the fits for each Wilson loop.

Loop	$-\langle \ln W_{RT} \rangle$	$\Delta[\ln W_{RT}]_{\text{MC}}$ ($\times 10^{-5}$)	$\Delta[\ln W_{RT}]_{\text{induced}}$ ($\times 10^{-5}$)
1×1	0.13976	2.2	—
1×2	0.24382	4.6	3.8
1×3	0.34158	7.9	5.3
2×2	0.39270	8.8	6.1
2×3	0.52235	13.7	8.1
3×3	0.66857	20.2	10.4

TABLE V: Comparison of simulation error and “induced” error (due to the uncertainty in the coupling in the perturbative expansion), for various Wilson loops, for the unimproved actions at $\beta = 16$ with $n_f = 1$.

Dependence on N ($\bar{\sigma} = 1.5$)			
c_n	$N = 4$	$N = 5$	$N = 6$
c_1	1.4334(6)	1.4334(6)	1.4334(6)
c_2	-1.37(4)	-1.37(4)	-1.37(4)
c_3	-0.91(56)	-0.91(56)	-0.91(56)
c_4	-0.1(15)	-0.1(15)	-0.1(15)
c_5	—	0.0(15)	0.0(15)
c_6	—	—	0.0(15)
$\chi_{\text{aug}}^2/\text{dof}$	0.56	0.56	0.56

Dependence on $\bar{\sigma}$ ($N = 6$)				
c_n	$\bar{\sigma} = 0.5$	$\bar{\sigma} = 1.0$	$\bar{\sigma} = 1.5$	$\bar{\sigma} = 5.0$
c_1	1.4338(4)	1.4335(5)	1.4334(6)	1.4333(6)
c_2	-1.40(3)	-1.38(4)	-1.37(4)	-1.36(4)
c_3	-0.49(38)	-0.79(51)	-0.91(56)	-0.98(77)
c_4	0.0(5)	-0.1(10)	0.0(15)	-0.5(50)
c_5	0.0(5)	0.0(10)	0.0(15)	0.0(50)
c_6	0.0(5)	0.0(10)	0.0(15)	0.0(50)
$\chi_{\text{aug}}^2/\text{dof}$	2.8	0.93	0.56	0.28

TABLE VI: Fit results for the 2×2 Wilson loop, for the “asqtad” actions with $n_f = 1$. The upper table shows the dependence of the results on the number of terms N in the fit, for a fixed prior width $\bar{\sigma} = 1.5$, while the lower table shows the dependence on $\bar{\sigma}$ for fixed $N = 6$. The augmented χ^2 per degree-of-freedom (dof) is also shown. The central values for the prior coefficients are $\bar{c}_n = 0$. Diagrammatic perturbation theory yields $c_1 = 1.4339(0)$, $c_2 = -1.400(2)$ and $c_3 = -0.52(7)$ [7]. More accurate Monte Carlo estimates of c_2 and c_3 are obtained in Sect. IV, using diagrammatic perturbation theory to constrain the lower-order terms.

D. Fitting and truncation errors

We use constrained curve fitting [28] in our fits to Eq. (2), which allows one to incorporate the assumption of a convergent perturbation series in a natural way; in particular, a large number of higher-order terms can be included in the fit, without spoiling the quality of the results for lower-order terms that can be resolved by the data.

Constrained curve fitting is motivated by Bayesian analysis; we refer the reader to Ref. [28] for an overview. In practice, we minimize an “augmented” least-squares

fit function χ_{aug}^2 , given by

$$\chi_{\text{aug}}^2 \equiv \chi^2 + \sum_{n=1}^N \frac{(c_n - \bar{c}_n)^2}{\bar{\sigma}_n^2}, \quad (20)$$

where χ^2 is the usual weighted sum-of-squared errors in fit to the Monte Carlo data, and N is the number of terms in the fit (cf. Eq. (2)), which we take to be larger than the order that we anticipate can be resolved by the data. Fitting the data with χ_{aug}^2 favors c_n 's in the interval $\bar{c}_n \pm \bar{\sigma}_n$, which are known collectively as ‘‘priors.’’

The values of \bar{c}_n and $\bar{\sigma}_n$ are to be chosen based on theoretical expectations. In the present case one expects that $c_n = O(1)$, if the perturbative expansion is convergent. We therefore take $\bar{c}_n = 0$, and use a single prior ‘‘width’’ for all orders, $\bar{\sigma}_n \equiv \bar{\sigma}$, which should be of $O(1)$. The optimal value for a prior such as $\bar{\sigma}$ can sometimes be determined from the data itself, by maximizing the probability of obtaining the data, given the prior information, as a function of the prior itself; this is the so-called ‘‘empirical’’ Bayes method (for details see Ref. [28]).

The sensitivity of the data to a given order in the expansion is reflected in the fit results; coefficients that are well determined by the data are relatively insensitive to changes in $\bar{\sigma}$ and in the number of terms N in the fit, while fit results for coefficients that are poorly or not at all constrained by the data simply reproduce the priors. We expect that the statistical quality of the simulation data here should allow for useful determinations of the three leading orders in the perturbative expansion.

To illustrate the quality of the constrained fits, some representative results are given in Table VI, here for the 2×2 Wilson loop for the ‘‘asqtad’’ actions with $n_f = 1$. The effects of varying the number of terms N in the fit, and of varying the prior width $\bar{\sigma}$, are shown. We see that the results for the three leading orders in the perturbative expansion, c_1 , c_2 , and c_3 , are very insensitive to the details of the priors, while the fit returns the prior information for the fourth- and higher-order terms, which simply indicates that the data are not accurate enough to resolve those terms, as anticipated.

The results for the three leading orders are in excellent agreement with diagrammatic perturbation theory, within the fit errors, of a few parts in 10^4 for c_1 , and a few percent for c_2 ; a reasonable NNLO signal $c_3 \approx -1$ is also obtained, which is remarkable, given how little *a priori* information went into the fit (more accurate results for c_2 and c_3 are obtained in Sect. IV, using diagrammatic perturbation theory to constrain the lower orders).

The results for the χ_{aug}^2 of the fits also suggest that an ‘‘optimal’’ prior width can be determined from the data, with $\bar{\sigma} \sim 1.0$ – 1.5 , which we also find using the optimization procedure given by the ‘‘empirical’’ Bayes method, alluded to above. Hence the simulation data are indeed consistent with the expectation that perturbation theory is reliable. For the rest of the fits in this paper we use $N = 6$, $\bar{c}_n = 0$, and $\bar{\sigma} = 1.5$.

IV. RESULTS

A. Fitting strategy

Simulation results for the perturbative coefficients of various Wilson loops are presented for the unimproved and ‘‘asqtad’’ actions in the next two subsections. The results are compared with a recent NNLO analysis using diagrammatic perturbation theory, which was done in the infinite-volume limit, and for zero quark mass, in Ref. [7].

We perform several types of fits for each set of actions. Fits are first done without input from diagrammatic perturbation theory for a given Wilson loop (though we always assume the relevant scales q_{RT}^* , as well as the coefficients for the 1×1 loop, in order to extract the numerical values of the α_V couplings from the simulation data). We then set the first-order coefficients to their values from diagrammatic perturbation theory, so as to improve the Monte Carlo estimates of the second- and third-order terms, and then we similarly constrain both the first- and second-order coefficients, so as to obtain the most accurate estimate possible of the third-order terms. This provides us with very stringent tests of the Monte Carlo method, and a very precise cross-check of the difficult NNLO diagrammatic calculations in Ref. [7].

For fits that use diagrammatic values to constrain lower-order coefficients, we computed the leading-order Feynman diagram loop integrals with TBC, for the 8^4 volume and quark masses that were used in the simulations, in order to consistently account for finite-volume and finite-mass effects in the simulation data. However these effects are negligible except for the largest Wilson loops and at the smallest couplings considered here [the leading finite-volume corrections are $\sim \alpha_V/\text{Vol} = O(10^{-4}) \times \alpha_V$, while the leading mass-dependent corrections are $\sim \alpha_V^2(m_0 a)^2 = O(0.01) \times \alpha_V^2$; see also Ref. [13] for an extensive finite-volume analysis in the pure-gauge Monte Carlo perturbation theory.]

We also plot the following three residuals

$$\kappa_1 \equiv \frac{1}{\alpha_V(q_{RT}^*)} \left[\frac{-\ln W_{RT}}{2(R+T)} \right], \quad (21)$$

$$\kappa_2 \equiv \frac{1}{\alpha_V^2(q_{RT}^*)} \left[\frac{-\ln W_{RT}}{2(R+T)} - c_{1;RT} \alpha_V \right], \quad (22)$$

and

$$\kappa_3 \equiv \frac{1}{\alpha_V^3(q_{RT}^*)} \left[\frac{-\ln W_{RT}}{2(R+T)} - c_{1;RT} \alpha_V - c_{2;RT} \alpha_V^2 \right], \quad (23)$$

which provide useful visualizations of the quality of the data (diagrammatic perturbation theory is used for the coefficients in κ_2 and κ_3). We plot the residuals versus the appropriate coupling $\alpha_V(q_{RT}^*)$, and in the limit of zero coupling one should find $\kappa_n \rightarrow c_n$ for the particular Wilson loop. Likewise a visible slope in the residual κ_n at small couplings reveals the sensitivity of the data to the next-order coefficient c_{n+1} .

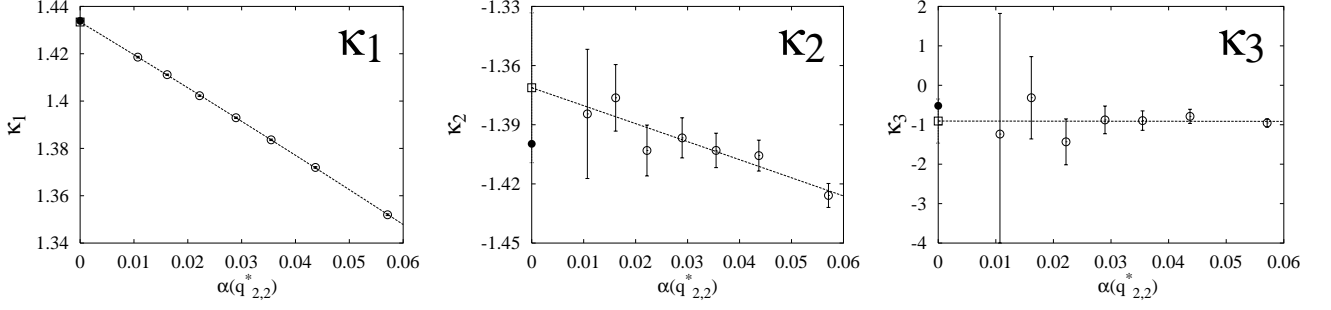


FIG. 7: Plots of the simulation results for κ_1 , κ_2 , and κ_3 , for the 2×2 Wilson loop, for the unimproved actions with $n_f = 1$. The simulation parameters are given in Table I. The intercepts marked by open squares (\square) in the plot for each κ_n give the results of the fits to the corresponding c_n , while the diagrammatic values [7] are indicated by filled circles (\bullet).

Number of flavours: $n_f = 1$						
Monte Carlo method				Diagrammatic values		
Loop	c_1	c_2	c_3	c_1	c_2	c_3
1×2	1.2038(4)	-1.327(29)	-1.26(46)	1.2039(0)	-1.335(0)	-1.10(3)
1×3	1.2586(5)	-1.253(36)	-1.43(56)	1.2589(0)	-1.277(1)	-0.95(6)
2×2	1.4334(6)	-1.368(39)	-0.95(59)	1.4339(0)	-1.400(2)	-0.52(8)
2×3	1.5163(7)	-1.281(47)	-1.11(71)	1.5172(0)	-1.351(3)	-0.26(12)
3×3	1.6080(8)	-1.230(56)	-0.45(82)	1.6090(0)	-1.298(6)	0.67(25)

Number of flavours: $n_f = 3$						
Monte Carlo method				Diagrammatic values		
Loop	c_1	c_2	c_3	c_1	c_2	c_3
1×2	1.2039(4)	-1.480(28)	-0.28(45)	1.2039(0)	-1.485(0)	-0.11(9)
1×3	1.2590(5)	-1.444(34)	-0.06(54)	1.2589(0)	-1.437(1)	0.02(11)
2×2	1.4337(5)	-1.529(38)	0.02(60)	1.4339(0)	-1.551(2)	0.51(13)
2×3	1.5169(6)	-1.476(46)	0.20(71)	1.5172(0)	-1.513(4)	0.73(16)
3×3	1.6088(8)	-1.431(53)	0.65(81)	1.6090(0)	-1.463(11)	1.62(30)

TABLE VII: Perturbative coefficients of various small Wilson loops for the unimproved actions, with $n_f = 1$, and with $n_f = 3$. The coefficients from diagrammatic perturbation theory [7] are compared with the results obtained from the Monte Carlo simulations. These fits to the Monte Carlo data used no diagrammatic input, except in the determination of the couplings for the expansion Eq. (2).

Diagrammatic input: c_1				
Loop	$n_f = 1$		$n_f = 3$	
	c_2	c_3	c_2	c_3
1×2	-1.332(9)	-1.19(22)	-1.480(10)	-0.28(25)
1×3	-1.270(11)	-1.20(27)	-1.434(12)	-0.19(30)
2×2	-1.403(12)	-0.48(29)	-1.541(13)	0.20(33)
2×3	-1.342(14)	-0.28(34)	-1.499(16)	0.52(39)
3×3	-1.292(17)	0.38(41)	-1.442(20)	0.80(46)

Diagrammatic input: $c_{1,2}$		
Loop	$n_f = 1$	$n_f = 3$
	c_3	c_3
1×2	-0.11(9)	-0.17(10)
1×3	0.02(11)	-0.12(11)
2×2	0.51(13)	0.42(13)
2×3	0.73(16)	0.81(16)
3×3	1.62(30)	1.16(27)

TABLE VIII: Monte Carlo results for perturbative coefficients for the unimproved actions, where in the left table the first-order term is set to its diagrammatic value, while in the right table both c_1 and c_2 are set to their diagrammatic values.

B. Unimproved actions

The unimproved actions were simulated for $n_f = 1$ and $n_f = 3$. The sensitivity of the data to three leading orders in the perturbative expansions is apparent in the plots of the three residuals κ_1 , κ_2 , and κ_3 , which are shown for a representative Wilson loop in Fig. 7. The

slope and curvature in the plot for κ_1 , for instance, indicate the sensitivity to c_2 and c_3 , while the fact that the plot for κ_3 has no noticeable slope indicates that the data are insensitive to c_4 , within the statistical errors.

Fit results for c_1 , c_2 , and c_3 , without input from diagrammatic perturbation theory (except for the couplings) are given in Table VII, for Wilson loops up to 3×3 . As

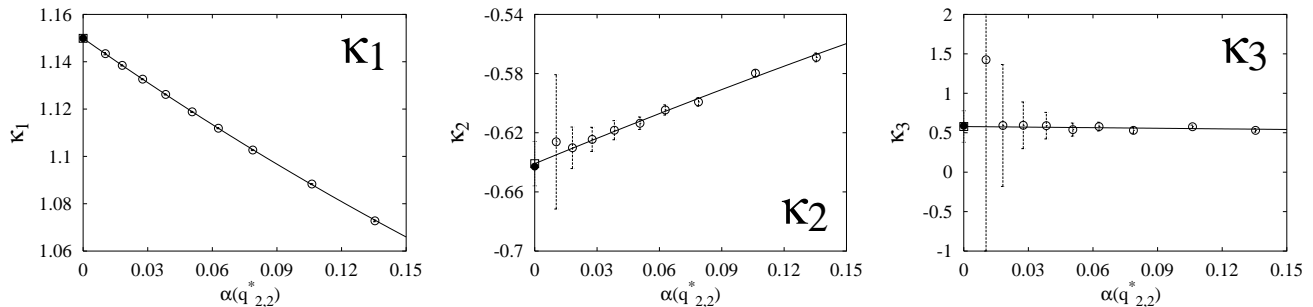


FIG. 8: Plots of κ_1 , κ_2 , and κ_3 for the 2×2 loop with the “asqtad” actions. Simulation parameters are given in Table III. The results of fits to the Monte Carlo data for the perturbative coefficients are indicated by open squares (\square), while the diagrammatic results are shown by filled circles (\bullet).

Monte Carlo method			Diagrammatic values			
Loop	c_1	c_2	c_3	c_1	c_2	c_3
1×2	0.9251(3)	-0.644(13)	0.20(18)	0.9252(0)	-0.646(0)	0.23(5)
1×3	0.9845(3)	-0.599(14)	0.37(19)	0.9845(0)	-0.595(1)	0.38(6)
2×2	1.1499(4)	-0.641(15)	0.58(20)	1.1499(0)	-0.643(2)	0.59(9)
2×3	1.2342(4)	-0.599(19)	0.88(26)	1.2341(0)	-0.595(3)	0.85(16)
3×3	1.3235(5)	-0.545(19)	1.16(23)	1.3235(0)	-0.522(4)	0.96(19)

Diagrammatic input: c_1		
Loop	c_2	c_3
1×2	-0.649(5)	0.26(12)
1×3	-0.600(6)	0.39(13)
2×2	-0.642(7)	0.59(14)
2×3	-0.594(7)	0.82(15)
3×3	-0.546(8)	1.17(17)

Diagrammatic input: $c_{1,2}$	
Loop	c_3
1×2	0.21(4)
1×3	0.28(5)
2×2	0.61(6)
2×3	0.84(8)
3×3	0.84(10)

TABLE IX: Perturbative coefficients for various small Wilson loops for the “asqtad” actions. There is no diagrammatic input in the Monte Carlo results in the left-most table (except for the couplings). In the middle table the Monte Carlo results are shown with the first-order term set to its diagrammatic value, while in the right-most table both c_1 and c_2 are set to their diagrammatic values.

discussed in Sect. IIID, excellent agreement with diagrammatic calculations is obtained, within the fit errors, which for c_1 are typically a few parts in 10^4 , and for c_2 are typically a few percent. The third order terms are also resolved, which is remarkable given that no diagrammatic input for these Wilson loops was used. The simulations also clearly resolve the perturbative dependence on the number of flavors, which in the case of c_2 shows a change of 3–4 standard deviations from $n_f = 1$ to $n_f = 3$.

The accuracy of the Monte Carlo results for the higher-order coefficients can be dramatically improved by further constraining the lower-order terms using available diagrammatic input. Results are shown in Table VIII where we first fix c_1 to its diagrammatic value, and then fix both c_1 and c_2 ; in the first case, the fit errors in c_2 and c_3 are reduced by factors of about 2–3 compared to the results in Table VII, while in the second case the errors in c_3 are reduced by a factor of about 5. Agreement with the diagrammatic values is obtained in all cases, within these greatly reduced errors, and in most cases the Monte Carlo results have errors that are comparable to those in the diagrammatic evaluations.

C. The “asqtad” actions

Our results for the perturbative expansions of Wilson loops for the “asqtad” actions are shown in Fig. 8, and in Table IX. The data is sensitive to the three leading

orders of the perturbative expansion, and the agreement with diagrammatic results is again impressive.

We note that the uncertainties in the coefficients obtained from these simulations are about a factor of 3 smaller than for the unimproved results presented in the preceding subsection, which owes to the fact that the “asqtad” simulations were done at larger couplings [the largest coupling for the unimproved simulations was $\alpha_V(q_{11}^*) \approx 0.06$, while for the “asqtad” simulations it was $\alpha_V(q_{11}^*) \approx 0.13$, cf. Tables I and III]. This fact should clearly be heeded in future studies, where one might work at still larger couplings, as long as the theory remains in the perturbative phase, as judged for example by simulation measurements of the Polyakov line, which provides an order parameter for confinement (a systematic approach to optimizing the choice of couplings is given in Refs. [13, 28]).

V. CONCLUSIONS AND OUTLOOK

Perturbative coefficients of Wilson loops were extracted from unquenched QCD simulations at weak couplings. Two sets of actions were analyzed: unimproved gluon and staggered-quark actions in one set, and $O(a^2)$ improved actions in the other. Simulations were also done for different numbers of dynamical fermions. An extensive analysis of systematic uncertainties was made; constrained-curve fitting in particular was used to extract

as much information as possible from the simulation data.

The Monte Carlo results for the perturbative coefficients were found to be in excellent agreement with calculations using diagrammatic perturbation theory, through next-to-next-to leading order. Results were obtained for the first-order coefficients with uncertainties of a few parts in 10^4 , while the second-order coefficients were obtained to a few-percent precision, without any input from diagrammatic perturbation theory (except for the perturbative expansion of the 1×1 plaquette, which was used to extract the relevant couplings $\alpha_V(q^*)$ from the simulation data). The results also show that the Monte Carlo perturbation theory is clearly sensitive to the number of dynamical fermion. Furthermore, when the two leading perturbative coefficients were constrained to their diagrammatic values, the third-order term was obtained with a precision comparable to that from the NNLO diagrammatic analysis [7], which required the evaluation of about fifty Feynman diagrams.

These results provide a stringent test of the Monte Carlo method as applied to highly-improved lattice actions with dynamical fermions, and also provide an important high-precision cross-check of the perturbation theory input to a recent determination of $\alpha_{\overline{\text{MS}}}(M_Z)$ by the HPQCD collaboration [2].

Remarkably little computational power was needed, since the simulations were done on small volumes (8^4), thanks to the use of twisted boundary conditions, which

eliminate lattice zero modes, and which suppress other finite-volume effects; the entire set of simulations for the “asqtad” actions only required the equivalent of about 60 months of run-time on a single 3 GHz processor. Larger lattices might be needed for other quantities, such as quark propagators [14], that are not as dominated by ultraviolet modes as the small Wilson loops analyzed here, though an earlier study for pure-gauge theories [13] found that finite-volume effects in such quantities could be removed by working on several relatively small volumes.

Additional work using this method is in progress, including the determination of the NNLO mass renormalization for the NRQCD heavy-quark action, and preliminary investigations of currents with infrared singularities.

Acknowledgments

We thank Peter Lepage, Christine Davies, and Matthew Nobes for fruitful conversations. We also thank Peter Lepage for providing us with his Bayesian-analysis software. We are grateful to Randy Lewis for providing resources including the use of his computer cluster at the University of Regina. Computations were also performed on facilities provided by WestGrid [32]. This work was supported in part by the Natural Sciences and Engineering Research Council of Canada.

-
- [1] C. T. H. Davies *et al.*, Phys. Rev. D **56**, 2755 (1997).
 [2] Q. Mason *et al.*, HPQCD Collaboration, Phys. Rev. Lett. **95**, 052002 (2005).
 [3] H. D. Trottier, Nucl. Phys. Proc. Suppl. **129**, 142 (2004).
 [4] Q. J. Mason, Ph.D. thesis, Cornell University (2004).
 [5] M. Lüscher and P. Weisz, Nucl. Phys. B **266**, 309 (1986).
 [6] M. Lüscher and P. Weisz, Nucl. Phys. B **452**, 234 (1995); B. Alles, M. Campostrini, A. Feo and H. Panagopoulos, Phys. Lett. B **324**, 433 (1994); B. Alles, A. Feo and H. Panagopoulos, Nucl. Phys. B **491**, 498 (1997); E. Follana and H. Panagopoulos, Phys. Rev. D **63**, 017501 (2001).
 [7] Q. Mason and H. D. Trottier, in preparation.
 [8] Q. Mason, H. D. Trottier, R. Horgan, C. T. H. Davies and G. P. Lepage, hep-ph/0511160.
 [9] G. P. Lepage, Phys. Rev. D **59**, 074502 (1999).
 [10] K. Symanzik, Nucl. Phys. B **226**, 187 (1983).
 [11] K. Orginos and D. Toussaint, Phys. Rev. D **59**, 014501 (1999); C. W. Bernard *et al.*, MILC Collaboration, Phys. Rev. D **64**, 054506 (2001).
 [12] W. C. Dimm, G. P. Lepage and P. B. Mackenzie, Nucl. Phys. Proc. Suppl. **42**, 403 (1995).
 [13] H. D. Trottier, N. H. Shakespeare, G. P. Lepage and P. B. Mackenzie, Phys. Rev. D **65**, 094502 (2002).
 [14] K. J. Juge, Nucl. Phys. Proc. Suppl. **94**, 584 (2001); **106**, 847 (2002).
 [15] A. Hart, R. R. Horgan and L. C. Storoni, Phys. Rev. D **70**, 034501 (2004).
 [16] Part of this work was presented in K. Y. Wong, Ph.D. thesis, Simon Fraser University, 2005.
 [17] F. Di Renzo *et al.*, Nucl. Phys. B **426**, 675 (1994).
 [18] F. Di Renzo and L. Scorzato, JHEP **0410**, 073, (2004).
 [19] G. 'tHooft, Nucl. Phys. B **153**, 141 (1979).
 [20] G. Parisi, LNF-84/4-P, Invited talk given at Summer Inst. Progress in Gauge Field Theory, Cargese, France, Sep 1-15 (1983).
 [21] R. Wohlert, DESY 87/069 (1987).
 [22] A. Gonzalez Arroyo and C. P. Korthals Altes, Nucl. Phys. B **311**, 433 (1988).
 [23] G. P. Lepage and P. B. Mackenzie, Phys. Rev. D **48**, 2250 (1993).
 [24] S. J. Brodsky, G. P. Lepage and P. B. Mackenzie, Phys. Rev. D **28**, 228 (1983).
 [25] I. Horvath, A. D. Kennedy and S. Sint, Nucl. Phys. Proc. Suppl. **73**, 834 (1999).
 [26] M. A. Clark and A. D. Kennedy, Nucl. Phys. Proc. Suppl. **129**, 850 (2004).
 [27] S. Gottlieb *et al.*, Phys. Rev. D **35**, 2531 (1987).
 [28] G. P. Lepage *et al.*, Nucl. Phys. Proc. Suppl. **106**, 12 (2002).
 [29] Y. Schröder, Phys. Lett. B **447**, 321 (1999).
 [30] We recomputed the leading-order Feynman diagram loop integrals here for finite-volume (8^4) TBC perturbation theory, and for the finite quark mass; see Sect. IV A.
 [31] M. G. Alford, W. Dimm, G. P. Lepage, G. Hockney and P. B. Mackenzie, Phys. Lett. B **361**, 87 (1995).
 [32] See <http://www.westgrid.ca/home.html>.